

# A systematic approach to CT evaluation of non-arthritic hip pain

Andrew J Curley<sup>1</sup>, Ethan R Ruh<sup>1</sup>, Amisha Shah<sup>2</sup>, Ashley E Disantis<sup>1</sup>, April Krivoniak<sup>2</sup>, Craig S Mauro<sup>1</sup> and Michael P McClincy<sup>1</sup>

<sup>1</sup>Department of Orthopedics, University of Pittsburgh Medical Center, Pittsburgh, Pennsylvania, USA

<sup>2</sup>Department of Radiology, University of Pittsburgh Medical Center, Pittsburgh, Pennsylvania, USA

Correspondence should be addressed to A J Curley

**Email**

[andrew.curley@](mailto:andrew.curley@americanhipinstitute.org)

[americanhipinstitute.org](http://americanhipinstitute.org)

- Bone morphology has been increasingly recognized as a significant variable in the evaluation of non-arthritic hip pain in young adults.
- Increased availability and use of multidetector CT in this patient population has contributed to better characterization of the osseous structures compared to traditional radiographs.
- Femoral and acetabular version, sites of impingement, acetabular coverage, femoral head–neck morphology, and other structural abnormalities are increasingly identified with the use of CT scan.
- In this review, a standard CT imaging technique and protocol is discussed, along with a systematic approach for evaluating pelvic CT imaging in patients with non-arthritic hip pain.

## Keywords

- ▶ computed tomography
- ▶ hip/thigh/pelvis
- ▶ femoroacetabular impingement

EFORT Open Reviews  
(2022) 7, 653–662

## Introduction

The field of hip preservation has undergone significant advancement since Ganz popularized femoroacetabular impingement syndrome (FAIS) two decades ago (1, 2). Since then, the understanding of non-arthritic hip pain, which includes a spectrum of diagnoses from instability to impingement, has been greatly enhanced by the use of advanced imaging modalities like CT and MRI. Simultaneously, there has been significant innovation in the clinical management of hip disorders, including advanced surgical techniques, that has led to improved outcomes and survivorship in this patient population.

Early studies on FAIS and hip instability were reported in the context of clinical examinations and plain radiographs (1, 2, 3). The implementation of MRI fostered another series of diagnostic advancements by providing a tool to assess the soft-tissue structures such as the labrum and cartilage (4, 5). However, osseous morphologic features, which MRI is unable to highlight, have been recently recognized as factors that can affect the clinical outcomes of patients with hip pain. These factors include extra-articular impingement, version and torsional morphologies of the acetabulum and/or femur, and subtle coverage abnormalities of the femoral head (6, 7, 8, 9, 10, 11, 12). These structural variables highlight the importance of using CT imaging to thoroughly evaluate the 3D bony anatomy of the femur and pelvis, and routine utilization of CT has

been endorsed by experts in the field of hip preservation (13). While a systematic approach has been described for assessing plain radiographs (14) and MRIs (15) of non-arthritic hip pain, a comprehensive diagnostic algorithm of CT imaging is less defined. Furthermore, consensus statements from a validated Delphi method were recently described for diagnostic imaging of FAIS (16, 17, 18). These experts agreed that radiographic evaluation should be used for initial assessment and MRI was considered the ‘gold standard’ in patients with FAIS; however, the role of CT imaging was less defined (18). Therefore, the purpose of this review is to provide a standardized imaging protocol and a systematic approach to interpreting CT sequences for patients with non-arthritic hip pain.

## CT scan protocol

CT scan is a cross-sectional imaging modality that uses radiation to provide increased image contrast resolution compared to radiographs, resulting in better visualization of bone structure. Multiplanar and 3D reformatting capabilities of CT scan can significantly improve the characterization of bony landmarks and morphology in contrast to 2D radiographic assessment. Additionally, reformatting enables CT to avoid many pitfalls of radiographs such as patient positioning and poor image quality.

At our institution, a 64-multi-detector CT scanner is utilized when obtaining non-arthritic hip CT images (Table 1). Patients are placed in a neutral supine position with the feet taped slightly inverted to ensure stability during the scan, specifically for quantification of the femoral version. Strategic padding and support are used to avoid any motion. The pelvis is scanned from the iliac crest to the lesser trochanter. To enable measurement of the femoral version, additional axial cuts are obtained from the distal 2 cm of the femoral condyles to the knee joints.

A disadvantage of CT is the increased dose of radiation, specifically for young individuals who have greater sensitivity to damage at the cellular level. The need for repetitive imaging of the pelvis can be especially concerning in children (19). Wylie *et al.* (20) noted that a pelvic CT for hip pain in young adults carried a 5–17 times greater relative risk for malignancy over their lifetime, albeit the absolute rate of malignancy was minimal (0.034–0.177%). To minimize radiation exposure, our scans utilize a low-dose technique with activation of Adaptive Statistical Iterative Reconstruction radiation dose-reducing software to reduce radiation dose by 30% on average. Depending on patient size and BMI, the average radiation dose for a pelvis CT scan for dysplasia ranges from 1.8 to 2.2 mSv, which is lower than a standard pelvis CT scan exposure of 3 mSv or more (21). Through dose reduction, pelvic CT scans demonstrate equivalent radiation exposure to a standard 3-view radiographic sequence of the pelvis (0.7 mSv per image) (22).

### Preparation for measurements on CT scan

A localizer is placed at the center of the femoral head on axial or coronal images. This point is referenced by corresponding scout lines on all the axial, sagittal, and coronal planes to confirm its central location on the femoral head. Thereafter, a best fit circle is drawn on the coronal image at the best image referenced by the localizer for axial and sagittal images (Fig. 1). A horizontal reference line is created by connecting a transverse line between the inferior aspect of each teardrops or ischium on the coronal image. A region 5 mm caudal to the roof of the acetabular

dome is localized, which typically corresponds to the 1:30 (anterosuperior) region of the acetabulum when viewed as a clockface (Fig. 2). All the measurements are performed with the digital caliper feature on Phillips iSite PACS system (Philips Healthcare).

### Acetabulum

#### Version

Acetabular version is commonly assessed as *central version* or *cranial version* on the axial images (Fig. 3). Central version is measured at the equator, or 3 o'clock position, of the acetabulum (23, 24, 25, 26). Differing methods have been reported for determining the location of cranial version, including 5 mm below the roof of the acetabulum (10, 23) or between the 1 and 2 o'clock positions (12, 26, 27). The authors prefer to utilize the former of these techniques, given its ease of use and reproducibility. Global acetabular version abnormalities often affect both central and cranial version, whereas focal anterior overcoverage may result in low cranial version with relatively normal central version (28).

#### Coverage

Initial cross-sectional measurements of femoral head coverage were recorded in the coronal and axial planes, though more sophisticated techniques have been recently described. The coronal metric most commonly utilized is the Wiberg center edge angle (W-CEA) (29), which is measured in the coronal sequence through the center of the femoral head. The W-CEA is formed by the angle consisting of lines through (1) the center of the femoral head and lateral edge of the sourcil, and (2) the horizontal reference line at the bottom of the ischium or teardrops. Recently, the Lisbon Agreement of FAIS imaging (16, 17, 18) defined that the W-CEA differs from the lateral center edge angle, which utilizes the most lateral bone-edge of the acetabulum rather than lateral edge of the sourcil (Fig. 4D). X-ray and CT measurements of center edge angle (CEA) have been shown to be similar, though Chadayammuri *et al.* (30) suggested that CT may result in slightly higher CEA values compared to standard X-ray (31). This finding is likely explained by the findings of Wylie *et al.*

**Table 1** Low dose CT scan protocol for non-arthritic hip pain.

Scan coverage and parameters	Planes, slice thickness, and algorithm	Reformats	3D reconstruction
<ul style="list-style-type: none"> <li>From iliac crest to lesser trochanter of femur.</li> <li>Voltage 100 kVp, Current 80–140 mA, pitch 0.98, table speed 39.37 mm/s, rotation time 0.8 s, detector coverage 40 mm.</li> </ul>	<ul style="list-style-type: none"> <li>Axial 1.25 mm bone plus</li> <li>Axial 1.25 mm standard</li> </ul>	<ul style="list-style-type: none"> <li>Pelvis coronal 2 mm bone plus</li> <li>Pelvis sagittal 2 mm bone plus</li> <li>Each hip – oblique axial in plane of femoral neck 2 mm bone plus</li> </ul>	<ul style="list-style-type: none"> <li>Surface rendered 3D reconstructions:</li> <li>Articulated pelvis with proximal femurs</li> <li>Isolated pelvis</li> <li>Isolated femurs</li> </ul>

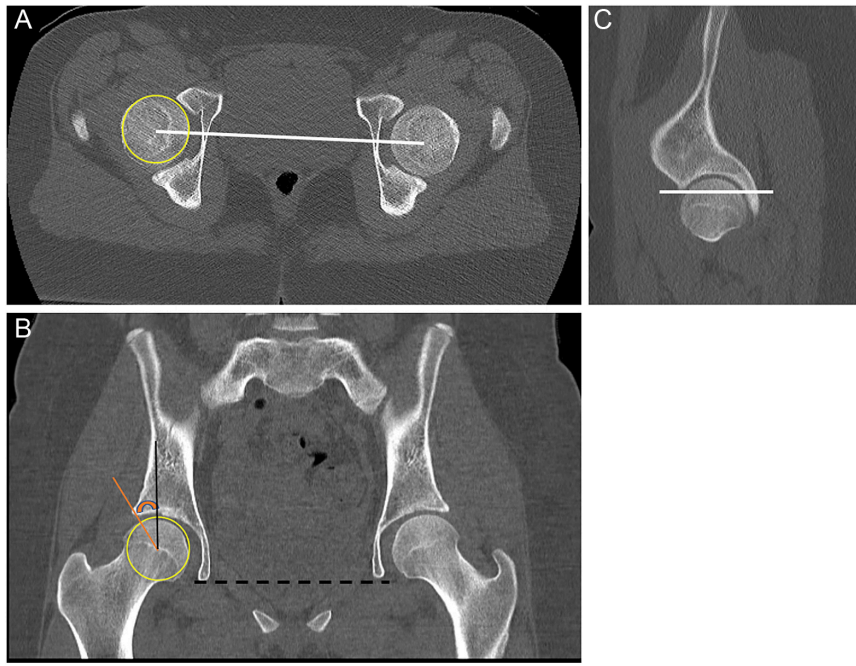


**Figure 1**  
 Definition of hip center and horizontal axis. The center of the femoral head is determined by a localizer placed at the center of the best fit circle of the femoral head on the axial or coronal image and referenced by scout lines on all axial, sagittal, and coronal planes (white lines seen on A and C). The best fit circle is then drawn on the coronal image determined by center of the femoral head referenced by the remaining planes (yellow circle on the right femoral head on B). The horizontal line touching both the teardrops (black dotted line) on the coronal image makes the transverse line required for the Wiberg center edge angle (W-CEA) and Tönnis angle measurements. W-CEA angle is measured on a single coronal reformatted image (B) where the best fit circle is drawn (yellow circle) determined by the center of the femoral head referenced from all the planes (A, C). The vertical line (black line) is 90° to the inter-teardrop horizontal line (black dotted line) on the same image, and the W-CEA is measured up to the lateral margin of the acetabular sourcil (orange angle). Acetabular landmarks noted at the geometric center of the femoral head (A) and at a point 5 mm caudal to the acetabular dome (B). Image C shows the 5 mm caudal line on the sagittal sequences. This line commonly intercepts the acetabulum at 1:30 when viewing the acetabulum as a clock face.

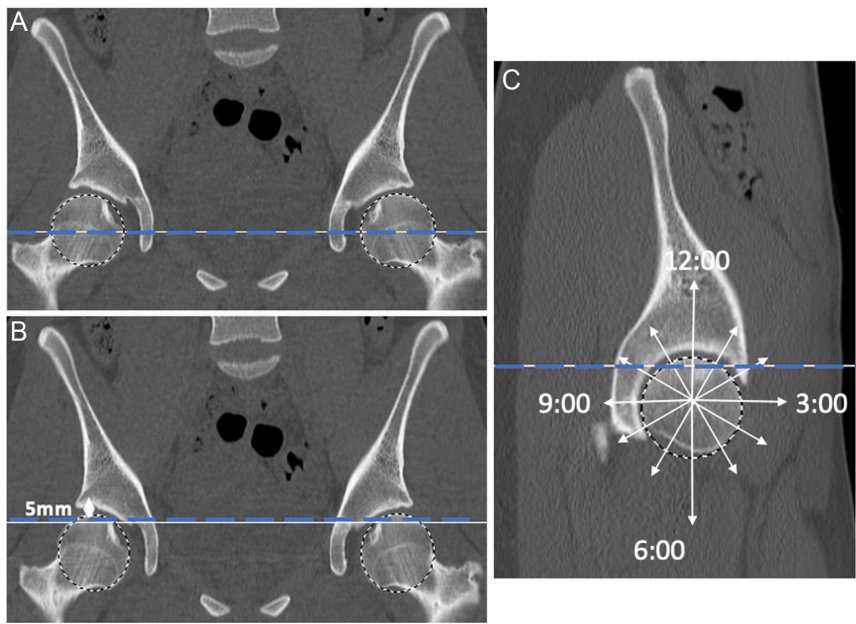


**Figure 2**  
 Definition of central and cranial acetabular measurement locations. Acetabular landmarks noted at the geometric center of the femoral head (A) and at a point 5 mm caudal to the acetabular dome (B). Image C shows the 5 mm caudal line on the sagittal sequences. This line commonly intercepts the acetabulum at 1:30 when viewing the acetabulum as a clock face.

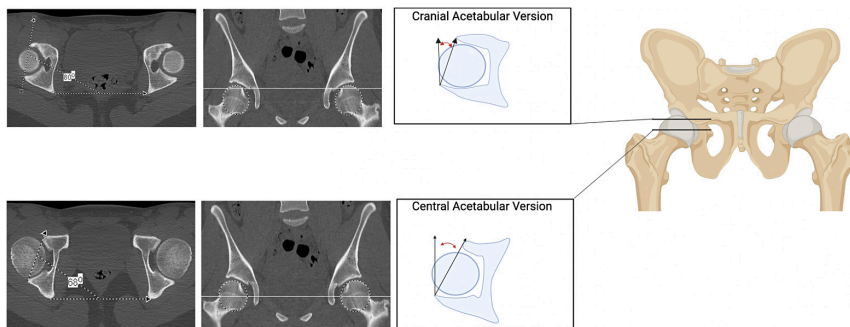


**Figure 3**  
Calculation of cranial and central acetabular version.

(32) who investigated the change in CEA measurements at the lateral acetabular *bone-edge* at varying locations, comparing radiographic measures to CT positions in 60 hips. The authors reported the CEA measurements at 1:00 (anterior acetabulum) mirrored those of the radiographic sourcil, while those taken at 12:00 mirrored those of the radiographic bone-edge. They concluded that the sourcil was a quantification of the acetabular coverage from the 1:00 to 2:00 corridor of the acetabulum, while the bone-edge was a quantification of focal acetabular coverage at 12:00. Our measurement protocol calculates the W-CEA at both the center of the femoral head and at the anterior acetabulum 5 mm below the roof of the acetabulum (Fig. 4). As noted previously, this anterior acetabular region typically falls between 1:00 and 2:00 on the clockface and is representative of anterosuperior coverage (32).

Using axial CT sequences, Anda *et al.* (33) popularized a method to determine anterior and posterior coverage of the femoral head with three metrics: anterior acetabular sector angle (AASA), posterior acetabular sector angle (PASA), and horizontal acetabular sector angle (HASA). The measurements are recorded on the axial sequence through the center of the femoral head, as detailed in

Fig. 5. These measurements are also performed at the cephalad acetabulum to account for variations in these regions, and we prefer measurements at 5 mm below the acetabular roof so as to record the cephalad sector angle measurement at the same location as cranial version. This typically corresponds closely to the 10 mm cephalad position originally described by Anda *et al.* (33).

To obtain a more comprehensive understanding of acetabular volume, Larson *et al.* (34) proposed a CT method to quantify femoral head coverage in multiple planes. Using radial reformatted CT slices for each clockface position on the acetabulum, a local coverage percentage can be calculated from the circumferential portion of the acetabular roof from the horizontal axis to the acetabular rim border point (Fig. 6). This technique allows for the analysis of acetabular coverage on the femoral head at locations that are in between the traditional superolateral, anterior, and posterior reference points (34). Nepple *et al.* (12) utilized this method to characterize three types of acetabular morphology in patients with acetabular dysplasia: anterosuperior, global, and posteriosuperior undercoverage.

Steppacher *et al.* (35) further scrutinized acetabular coverage, distinguishing the cotyloid fossa from the

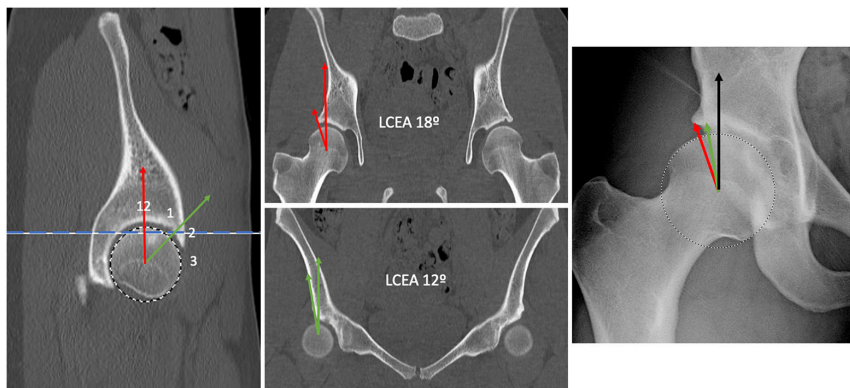


**Figure 4**  
Center edge angle (CEA) measurements at *bone-edge* and *sourcil-edge*. Sagittal slice through the center of the femoral head (A), with a transverse blue line depicting the cranial position 5 mm below the acetabular dome that aligns with the sourcil edge. The red line at 12:00 depicts the location of the CEA at the *bone-edge* (B), whereas the green line correlates with the typical location between 1:00 and 2:00 of CEA at the *sourcil-edge* (C) as demonstrated by Wylie *et al.* (29). Anteroposterior hip radiograph (D) demonstrating the locations of the *bone-edge* (red line) and *sourcil-edge* relative to a vertical reference line (black line). According to the Lisbon Agreement (16, 17, 18), the Wiberg center edge angle (W-CEA) would measure the *sourcil-edge* (D, green line);, whereas the lateral center edge (L-CEA) would utilize the *bone-edge* (D, red line).

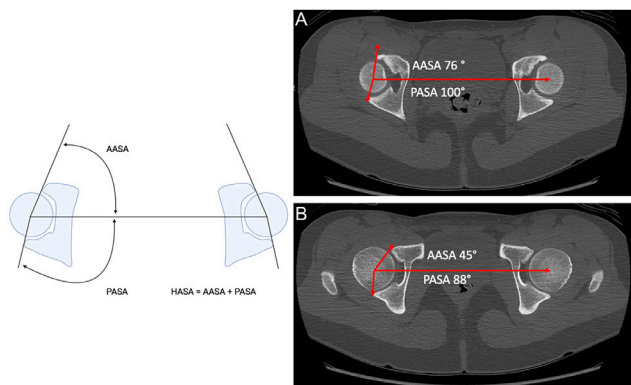


**Figure 5**

Acetabular sector angle measurements at cranial (A) and central (B) acetabulum. Anterior acetabular sector angle (AASA), posterior acetabular sector angle (PASA), and horizontal acetabular sector angle (HASA).

lunate surface of articular cartilage. Radial reformatted axial oblique slices through the center of the femoral head are utilized to create 14 different positions along the clockface of the acetabulum. At each location, the inner and outer center edge angles are used to quantify the size and shape of the lunate surface. Pun *et al.* (36) utilized this methodology to characterize two types of pincer impingement: increased anterior and posterior lunate surface widths (Type 1) and larger fossa size without increased anterior and posterior lunate surface widths (Type 2). These authors proposed that Type 1 pincer hips may be more amenable to rim trimming and Type 2 pincer hips would be better addressed with a reverse periacetabular osteotomy (PAO).

*Anterior inferior iliac spine/subspine*

Hetsroni *et al.* (6, 37) classified anterior inferior iliac spine (AIIS)/subspine morphology relative to the location of the acetabular rim, suggesting that extra-articular hip impingement may be associated with subspine variants that span farther distally. While originally described on false-profile radiographs, subspine abnormalities can be assessed on reformatted 3D CT images (Fig. 7) (38). Recent evidence suggests that, in comparison to 3D CT images, MRI was unreliable in characterizing the subspine morphology (39).

**Femur**

*Femoral head-neck junction*

In an early study of the femoral head-neck junction, Nötzli *et al.* (40) used an axial oblique slice at the center of the femoral head to measure the alpha angle, noting cam deformities at greater than 50°. However, this single axial oblique slice, which was limited to detecting cam lesions at the 3 o'clock position, was unable to assess a common location for abnormalities at the 1- to 2 o'clock positions (41, 42). To address this issue, subsequent studies employed radial plane images formatted around the femoral neck axis to circumferentially evaluate the femoral head-neck junction, including the anterosuperior quadrant (Fig. 8) (41, 42, 43). The circumferential evaluation of the femoral head-neck junction aids in planning cam resection and femoral osteoplasty.

Femoral head-neck offset (FHNO), popularized by Eijer *et al.* (44), is another metric to assess for abnormal morphology that can also be measured on radial plane

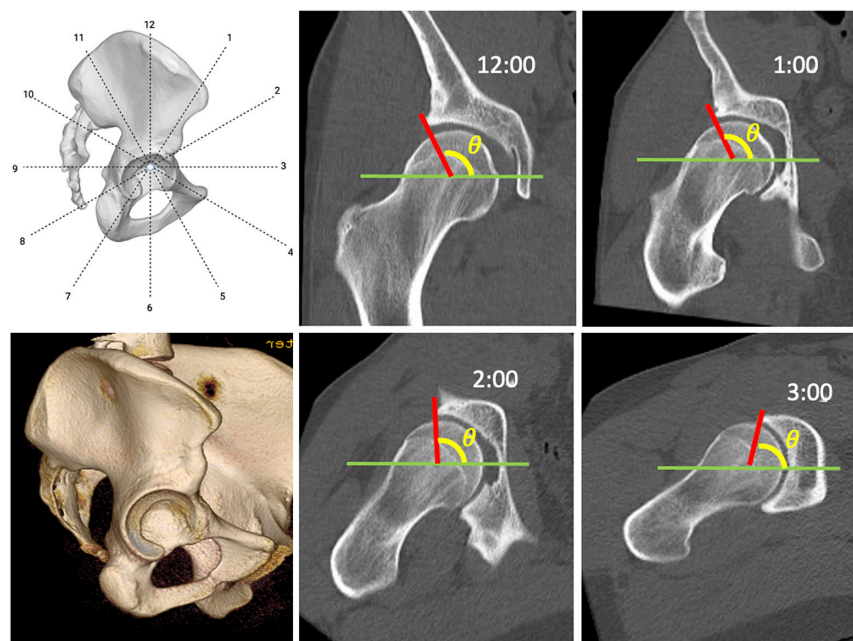


**Figure 6**

Radial reformatted CT slices for each clockface position on the acetabulum as described by Larson *et al.* (31). These images can be used to calculate a local coverage percentage (C%) from the circumferential portion of the acetabular roof, which can be determined as angle ( $\theta$ ) from the horizontal axis (green line) to the acetabular rim border point (red line). Local coverage percentage is calculated from the equation:  $C\% = \theta / 180^\circ \times 100$ .

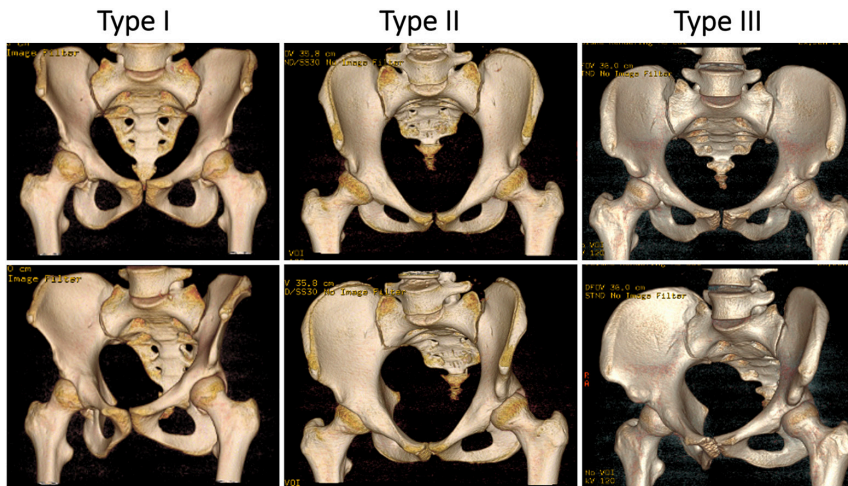


**Figure 7**  
Anterior inferior iliac spine (AIIS) morphology classification as defined by Hetsroni *et al.* (34). The most inferior aspect of the AIIS is located above (Type I), at the same level (Type II), or below (Type III) the acetabular rim.

images (45). FHNO can be utilized to quantify global shift of the femoral head relative to the femoral neck, which differs from a focal prominence in the head–neck region. Furthermore, FHNO can be normalized to a patient’s anatomy by calculating the FHNO ratio (FHNO divided by radius of the femoral head), which was initially described to mitigate differences in radiographic magnification (44, 46).

*Version/torsion*

The impact of the femoral version on hip function and pathology has become increasingly recognized in the past decade (10, 11). A recent cross-sectional study of 538 symptomatic hips suggested an incidence of severe femoral version abnormalities in 17% of patients (10). As described by Murphy *et al.* (47), the femoral version is measured as the angle between two lines: (1) the center of the femoral head to the center of the femoral neck at its base and (2) the posterior femoral condylar axis (Fig. 9) (48). Recent interest has focused on identifying the location where a femoral torsional abnormality occurs, as this may guide treatment for determining the site where derotational osteotomy

should be performed (49, 50). To evaluate whether a torsional abnormality occurs in the supratrochanteric or infratrochanteric region, Kim *et al.* (49) measured a line at the intertrochanteric axis in addition to the two traditional lines used for the femoral version. Using this methodology, Waisbrod *et al.* (50) reported that femoral torsion is most frequently located in the infratrochanteric region, rather than the supratrochanteric region.

To quantify the contribution of the hip abductors in the axial plane, Batailler *et al.* (51) proposed three new measurements to determine the position of the greater trochanter: (1) functional antetorsion, (2) posterior tilt, and (3) posterior translation of the greater trochanter. Using the first axial slice through the superior aspect of the femoral neck, a line is made through the axis of the greater trochanter, connecting the most lateral point of the anterior facet and the most posterior edge of the greater trochanter. This axis of the greater trochanter, along with the femoral neck axis (as defined by Murphy *et al.* (47)), are utilized to define functional antetorsion, posterior tilt, and posterior translation of the greater trochanter as demonstrated in Fig. 10. For preoperative

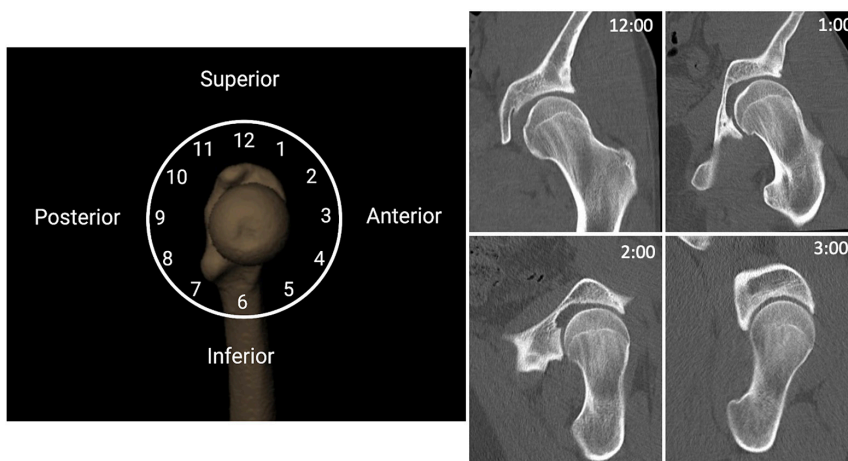


**Figure 8**  
Radial plane images are reformatted circumferentially around the center of the femoral neck axis, allowing for evaluation of the femoral head–neck junction at each location on the clock face.

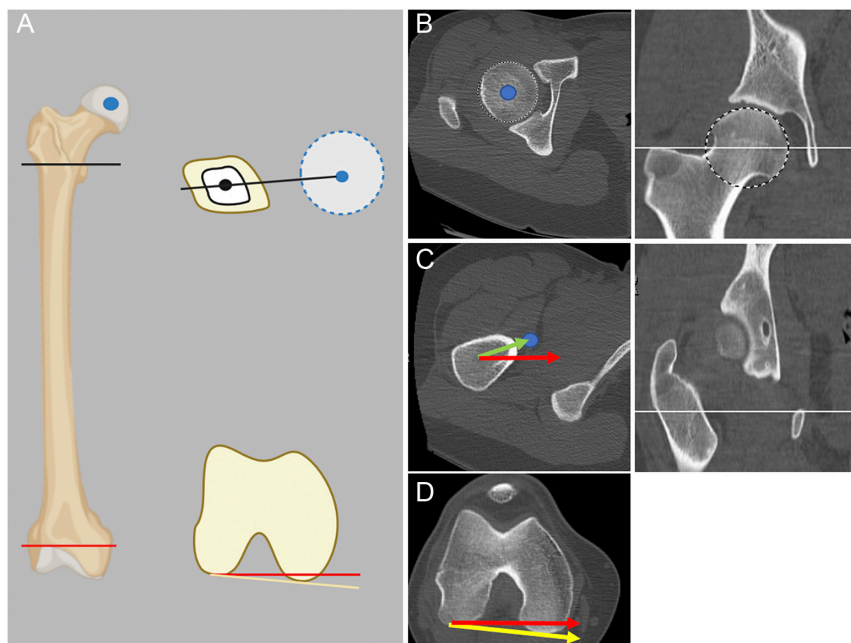


**Figure 9**

Femoral version measurement (A) as described by Murphy *et al.* (43). Axial slices are used to identify the femoral neck axis (green line), drawn from a line connecting the center of the femoral head depicted by the blue dot (B) and base of the femoral neck (C). An additional slice through the distal femur (D) is used to identify the posterior femoral condylar axis (yellow line). Femoral version is calculated as the summation of the angles created by the femoral neck axis and posterior condylar axis, relative to a horizontal reference line (red line).

planning of a femoral rotational osteotomy, the authors concluded that these metrics can help position the greater trochanter appropriately in the axial plane, resulting in normal functional antetorsion (51).

### CT for preoperative planning

CT scan has recently gained an increasing role in preoperative planning for non-arthritic hip disorders.

Rapid technical advancements in the field of automation software for multiplanar imaging modalities like 3D CT scan have introduced a wide range of new capabilities including automated anatomic measurements and virtual surgical planning (Fig. 11) (52). These approaches allow one to measure radiographic parameters in real-time before and after virtual surgical interventions, including osteotomies and osteoplasties. The introduction of 3D printing of CT-derived anatomy allows for hands-on

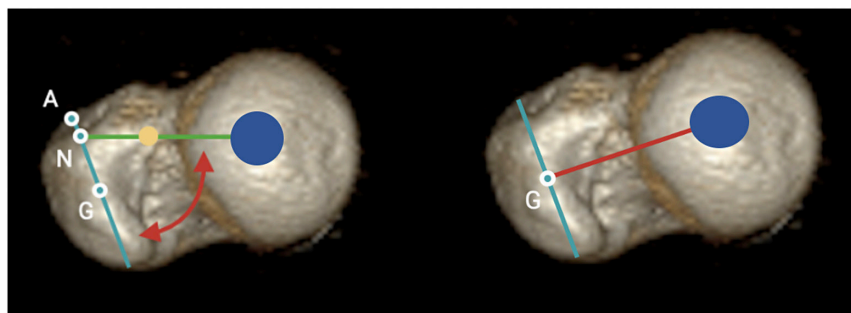


**Figure 10**

Measurement of functional antetorsion, posterior tilt, and posterior translation as described by Batailler *et al.* (47). The greater axis of the greater trochanter (teal line) connects the anterior (point A) and posterior aspects of the greater trochanter, with the midpoint of this line depicted by point G. The femoral neck axis (green line) connects the center of the femoral head (blue dot) and base of the femoral neck (yellow dot), intersecting the greater axis of the greater trochanter at point N. Posterior tilt (red arrow) is the angle between the femoral neck axis and the greater axis of the greater trochanter. Posterior translation is the ratio of lines AN to AG (AN/AG). Functional antetorsion is measured by the difference between the posterior condylar axis and a line connecting the center of the femoral head with the center of the greater axis of the greater trochanter (red line). While these images are demonstrated on 3D reconstructions for clarity, the measurements are performed on an axial slice through the top of the greater trochanter.

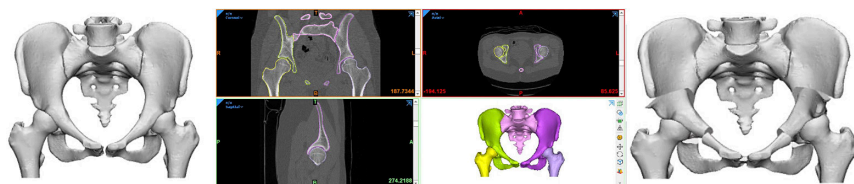


**Figure 11**

Virtual software, utilizing data from CT imaging, can be utilized for preoperative surgical planning of peri-acetabular osteotomies.

understanding of the bony morphology which also aids in surgical decision-making (53). While the details of these advanced techniques are beyond the scope of this article, their prospect is certainly noteworthy.

## Conclusion

As the field of hip preservation continues to evolve, the contributions of structural factors of the hip on clinical outcomes have been increasingly recognized. Building upon 2D plain radiographs, CT imaging has helped to comprehend the 3D osseous structure of the hip, advancing the management of non-arthritic hip pain. Future directions of hip diagnostics will aim to translate these static 3D images into a dynamic assessment of hip kinematics, possibly through computer software simulations and/or dynamic *in vivo* imaging.

### ICMJE Conflict of Interest Statement

The authors declare that there is no conflict of interest that could be perceived as prejudicing the impartiality of the research reported.

### Funding Statement

This study did not receive any specific grant from any funding agency in the public, commercial or not-for-profit sector.

## References

- Ganz R, Parvizi J, Beck M, Leunig M, Nötzli H & Siebenrock KA. Femoroacetabular impingement: a cause for osteoarthritis of the hip. *Clinical Orthopaedics and Related Research* 2003 **417** 112–120. (<https://doi.org/10.1097/01.blo.0000096804.78689.c2>)
- Beck M, Kalhor M, Leunig M & Ganz R. Hip morphology influences the pattern of damage to the acetabular cartilage: femoroacetabular impingement as a cause of early osteoarthritis of the hip. *Journal of Bone and Joint Surgery: British Volume* 2005 **87** 1012–1018. (<https://doi.org/10.1302/0301-620X.87B7.15203>)
- Murphy SB, Ganz R & Müller ME. The prognosis in untreated dysplasia of the hip. A study of radiographic factors that predict the outcome. *Journal of Bone and Joint Surgery: American Volume* 1995 **77** 985–989. (<https://doi.org/10.2106/00004623-199507000-00002>)
- Mintz DN, Hooper T, Connell D, Buly R, Padgett DE & Potter HG. Magnetic resonance imaging of the hip: detection of labral and chondral abnormalities using noncontrast imaging. *Arthroscopy* 2005 **21** 385–393. (<https://doi.org/10.1016/j.arthro.2004.12.011>)
- Edwards DJ, Lomas D & Villar RN. Diagnosis of the painful hip by magnetic resonance imaging and arthroscopy. *Journal of Bone and Joint Surgery: British Volume* 1995 **77** 374–376. (<https://doi.org/10.1302/0301-620X.77B3.7744918>)
- Hetsroni I, Larson CM, Dela Torre K, Zbeda RM, Magennis E & Kelly BT. Anterior inferior iliac spine deformity as an extra-articular source for hip impingement: a series of 10 patients treated with arthroscopic decompression. *Arthroscopy* 2012 **28** 1644–1653. (<https://doi.org/10.1016/j.arthro.2012.05.882>)
- Sa D de, Alradwan H, Cargnelli S, Thawer Z, Simunovic N, Cadet E, Bonin N, Larson C & Ayeni OR. Extra-articular hip impingement: a systematic review examining operative treatment of psoas, subspine, ischiofemoral, and greater trochanteric/pelvic impingement. *Arthroscopy* 2014 **30** 1026–1041. (<https://doi.org/10.1016/j.arthro.2014.02.042>)
- Stafford GH & Villar RN. Ischiofemoral impingement. *Journal of Bone and Joint Surgery: British Volume* 2011 **93** 1300–1302. (<https://doi.org/10.1302/0301-620X.93B10.26714>)
- Safran MR. Microinstability of the hip – gaining acceptance. *Journal of the American Academy of Orthopaedic Surgeons* 2019 **27** 12–22. (<https://doi.org/10.5435/JAAOS-D-17-00664>)
- Lerch TD, Todorski IAS, Steppacher SD, Schmaranzer F, Werlen SF, Siebenrock KA & Tannast M. Prevalence of femoral and acetabular version abnormalities in patients with symptomatic hip disease: a controlled study of 538 hips. *American Journal of Sports Medicine* 2018 **46** 122–134. (<https://doi.org/10.1177/0363546517726983>)
- Wang CK, Cohen D, Kay J, Almasri M, Simunovic N, Cardenas-Nylander C, Ranawat AS & Ayeni OR. The effect of femoral and acetabular version on outcomes following hip arthroscopy: a systematic review. *Journal of Bone and Joint Surgery: American Volume* 2022 **104** 271–283. (<https://doi.org/10.2106/JBJS.21.00375>)
- Nepple JJ, Wells J, Ross JR, Bedi A, Schoenecker PL & Clohisy JC. Three patterns of acetabular deficiency are common in young adult patients with acetabular dysplasia. *Clinical Orthopaedics and Related Research* 2017 **475** 1037–1044. (<https://doi.org/10.1007/s11999-016-5150-3>)
- McClincy MP, Wylie JD, Williams DN & Novais EN. Standardizing the diagnostic evaluation of nonarthritic hip pain through the Delphi method. *Orthopaedic Journal of Sports Medicine* 2021 **9** 2325967121991213. (<https://doi.org/10.1177/2325967121991213>)
- Clohisy JC, Carlisle JC, Beaulé PE, Kim YJ, Trousdale RT, Sierra RJ, Leunig M, Schoenecker PL & Millis MB. A systematic approach to the plain radiographic evaluation of the young adult hip. *Journal of Bone and Joint Surgery: American Volume* 2008 **90** (Supplement 4) 47–66. (<https://doi.org/10.2106/JBJS.H.00756>)
- Lewis PB, Weber AE, Kuhns BD & Nho SJ. A systematic approach to magnetic resonance imaging interpretation of sports medicine injuries of the hip. *JBJS Reviews* 2018 **6** e6. (<https://doi.org/10.2106/JBJS.RVW.17.00204>)
- Mascarenhas VV, Castro MO, Rego PA, Sutter R, Sconfienza LM, Kassarian A, Schmaranzer F, Ayeni OR, Dietrich TJ, Robinson P, et al. The Lisbon Agreement on femoroacetabular impingement imaging – part 1: overview. *European Radiology* 2020 **30** 5281–5297. (<https://doi.org/10.1007/s00330-020-06822-9>)
- Mascarenhas VV, Castro MO, Afonso PD, Rego P, Dienst M, Sutter R, Schmaranzer F, Sconfienza L, Kassarian A, Ayeni OR, et al. The Lisbon Agreement on femoroacetabular impingement imaging – part 2: general issues, parameters, and

reporting. *European Radiology* 2021 **31** 4634–4651. (<https://doi.org/10.1007/s00330-020-07432-1>)

**18. Castro MO, Mascarenhas VV, Afonso PD, Rego P, Schmaranzer F, Sutter R, Kassirjian A, Sconfienza L, Dienst M, Ayeni OR, et al.** The Lisbon Agreement on femoroacetabular impingement imaging – part 3: imaging techniques. *European Radiology* 2021 **31** 4652–4668. (<https://doi.org/10.1007/s00330-020-07501-5>)

**19. Pearce MS, Salotti JA, Little MP, McHugh K, Lee C, Kim KP, Howe NL, Ronckers CM, Rajaraman P, Sir Craft AW, et al.** Radiation exposure from CT scans in childhood and subsequent risk of leukaemia and brain tumours: a retrospective cohort study. *Lancet* 2012 **380** 499–505. ([https://doi.org/10.1016/S0140-6736\(12\)60815-0](https://doi.org/10.1016/S0140-6736(12)60815-0))

**20. Wylie JD, Jenkins PA, Beckmann JT, Peters CL, Aoki SK & Maak TG.** Computed tomography scans in patients with young adult hip pain carry a lifetime risk of malignancy. *Arthroscopy* 2018 **34** 155.e3–163.e3. (<https://doi.org/10.1016/j.arthro.2017.08.235>)

**21. Kanal KM, Butler PF, Chatfield MB, Wells J, Samei E, Simanowith M, Golden D, Gress DA, Burleson J, Sensakovic WF, et al.** U.S. diagnostic reference levels and achievable doses for 10 pediatric CT examinations. *Radiology* 2022 **302** 164–174. (<https://doi.org/10.1148/radiol.2021211241>)

**22. Hart D & Wall BF.** UK population dose from medical X-ray examinations. *European Journal of Radiology* 2004 **50** 285–291. ([https://doi.org/10.1016/S0720-048X\(03\)00178-5](https://doi.org/10.1016/S0720-048X(03)00178-5))

**23. Jamali AA, Mladenov K, Meyer DC, Martinez A, Beck M, Ganz R & Leunig M.** Anteroposterior pelvic radiographs to assess acetabular retroversion: high validity of the 'cross-over-sign'. *Journal of Orthopaedic Research* 2007 **25** 758–765. (<https://doi.org/10.1002/jor.20380>)

**24. Abel MF, Sutherland DH, Wenger DR & Mubarak SJ.** Evaluation of CT scans and 3-D reformatted images for quantitative assessment of the hip. *Journal of Pediatric Orthopedics* 1994 **14** 48–53. (<https://doi.org/10.1097/01241398-199401000-00011>)

**25. Tönnis D & Heinecke A.** Acetabular and femoral anteversion: relationship with osteoarthritis of the hip. *Journal of Bone and Joint Surgery: American Volume* 1999 **81** 1747–1770. (<https://doi.org/10.2106/00004623-199912000-00014>)

**26. Ross JR, Nepple JJ, Philippon MJ, Kelly BT, Larson CM & Bedi A.** Effect of changes in pelvic tilt on range of motion to impingement and radiographic parameters of acetabular morphologic characteristics. *American Journal of Sports Medicine* 2014 **42** 2402–2409. (<https://doi.org/10.1177/0363546514541229>)

**27. Zaltz I, Kelly BT, Hetsroni I & Bedi A.** The crossover sign overestimates acetabular retroversion. *Clinical Orthopaedics and Related Research* 2013 **471** 2463–2470. (<https://doi.org/10.1007/s11999-012-2689-5>)

**28. Perreira AC, Hunter JC, Laird T & Jamali AA.** Multilevel measurement of acetabular version using 3-D CT-generated models: implications for hip preservation surgery. *Clinical Orthopaedics and Related Research* 2011 **469** 552–561. (<https://doi.org/10.1007/s11999-010-1567-2>)

**29. Wiberg G.** Studies on dysplastic acetabula and congenital subluxation of the hip joint with special reference to the complication of osteoarthritis. *JAMA* 1940 **115** 81.

**30. Chadayammuri V, Garabekyan T, Jesse MK, Pascual-Garrido C, Strickland C, Milligan K & Mei-Dan O.** Measurement of lateral acetabular coverage: a comparison between CT and plain radiography. *Journal of Hip Preservation Surgery* 2015 **2** 392–400. (<https://doi.org/10.1093/jhps/hnv063>)

**31. Monazzam S, Bomar JD, Cidambi K, Kruk P & Hosalkar H.** Lateral center-edge angle on conventional radiography and computed tomography. *Clinical Orthopaedics and Related Research* 2013 **471** 2233–2237. (<https://doi.org/10.1007/s11999-012-2651-6>)

**32. Wylie JD, Kapron AL, Peters CL, Aoki SK & Maak TG.** Relationship between the lateral center-edge angle and 3-dimensional acetabular coverage. *Orthopaedic Journal of Sports Medicine* 2017 **5** 2325967117700589. (<https://doi.org/10.1177/2325967117700589>)

**33. Anda S, Svenningsen S, Dale LG & Benum P.** The acetabular sector angle of the adult hip determined by computed tomography. *Acta Radiologica: Diagnosis* 1986 **27** 443–447. (<https://doi.org/10.1177/028418518602700415>)

**34. Larson CM, Moreau-Gaudry A, Kelly BT, Thomas Byrd JW, Tonetti J, Lavallee S, Chabanas L, Barrier G & Bedi A.** Are normal hips being labeled as pathologic? A CT-based method for defining normal acetabular coverage. *Clinical Orthopaedics and Related Research* 2015 **473** 1247–1254. (<https://doi.org/10.1007/s11999-014-4055-2>)

**35. Steppacher SD, Lerch TD, Gharanzadeh K, Liechti EF, Werlen SF, Puls M, Tannast M & Siebenrock KA.** Size and shape of the lunate surface in different types of pincer impingement: theoretical implications for surgical therapy. *Osteoarthritis and Cartilage* 2014 **22** 951–958. (<https://doi.org/10.1016/j.joca.2014.05.010>)

**36. Pun SY, Hingsammer A, Millis MB & Kim YJ.** Is increased acetabular cartilage or fossa size associated With pincer femoroacetabular impingement? *Clinical Orthopaedics and Related Research* 2017 **475** 1013–1023. (<https://doi.org/10.1007/s11999-016-5063-1>)

**37. Hetsroni I, Poultides L, Bedi A, Larson CM & Kelly BT.** Anterior inferior iliac spine morphology correlates with hip range of motion: a classification system and dynamic model. *Clinical Orthopaedics and Related Research* 2013 **471** 2497–2503. (<https://doi.org/10.1007/s11999-013-2847-4>)

**38. Curley AJ, Owens JS, Jimenez AE, Maldonado DR, Saks BR, Sabetian PW, Lall AC & Domb BG.** Arthroscopic subspine decompression is commonly reported in a heterogenous patient population with concomitant procedures: a systematic review. *Arthroscopy* 2022 **38** 2529–2542. (<https://doi.org/10.1007/s00167-022-07108-x>)

**39. Efrima B, Amar E, Ovadia JE, Levy O, Ben Yehuda O & Rath E.** Magnetic resonance imaging is not reliable in classifying anterior inferior iliac spine morphology compared to 3-dimensional computerized tomography. *Arthroscopy* 2022 **38** 793–798. (<https://doi.org/10.1016/j.arthro.2021.06.007>)

**40. Nötzli HP, Wyss TF, Stoecklin CH, Schmid MR, Treiber K & Hodler J.** The contour of the femoral head-neck junction as a predictor for the risk of anterior impingement. *Journal of Bone and Joint Surgery: British Volume* 2002 **84** 556–560. (<https://doi.org/10.1302/0301-620x.84b4.12014>)

**41. Rakhra KS, Sheikh AM, Allen D & Beaulé PE.** Comparison of MRI alpha angle measurement planes in femoroacetabular impingement. *Clinical Orthopaedics and Related Research* 2009 **467** 660–665. (<https://doi.org/10.1007/s11999-008-0627-3>)

**42. Nepple JJ, Martel JM, Kim YJ, Zaltz I, Clohisy JC & ANCHOR Study Group.** Do plain radiographs correlate with CT for imaging of cam-type femoroacetabular impingement? *Clinical Orthopaedics and Related Research* 2012 **470** 3313–3320. (<https://doi.org/10.1007/s11999-012-2510-5>)

**43. Beaulé PE, Zaragoza E, Motamedi K, Copelan N & Dorey FJ.** Three-dimensional computed tomography of the hip in the assessment of femoroacetabular impingement. *Journal of Orthopaedic Research* 2005 **23** 1286–1292. (<https://doi.org/10.1016/j.orthres.2005.03.011.1100230608>)

**44. Eijer H, Myers SR & Ganz R.** Anterior femoroacetabular impingement after femoral neck fractures. *Journal of Orthopaedic Trauma* 2001 **15** 475–481. (<https://doi.org/10.1097/00005131-200109000-00003>)

**45. Wells J, Nepple JJ, Crook K, Ross JR, Bedi A, Schoenecker P & Clohisy JC.** Femoral morphology in the dysplastic hip: three-dimensional characterizations With CT. *Clinical Orthopaedics and Related Research* 2017 **475** 1045–1054. (<https://doi.org/10.1007/s11999-016-5119-2>)

- 46. Peelle MW, Della Rocca GJ, Maloney WJ, Curry MC & Clohisy JC.** Acetabular and femoral radiographic abnormalities associated with labral tears. *Clinical Orthopaedics and Related Research* 2005 **441** 327–333. (<https://doi.org/10.1097/01.blo.0000181147.86058.74>)
- 47. Murphy SB, Simon SR, Kijewski PK, Wilkinson RH & Griscom NT.** Femoral anteversion. *Journal of Bone and Joint Surgery: American Volume* 1987 **69** 1169–1176. (<https://doi.org/10.2106/00004623-198769080-00010>)
- 48. Schmaranzer F, Lerch TD, Siebenrock KA, Tannast M & Steppacher SD.** Differences in femoral torsion among various measurement methods increase in hips with excessive femoral torsion. *Clinical Orthopaedics and Related Research* 2019 **477** 1073–1083. (<https://doi.org/10.1097/CORR.0000000000000610>)
- 49. Kim HY, Lee SK, Lee NK & Choy WS.** An anatomical measurement of medial femoral torsion. *Journal of Pediatric Orthopedics: Part B* 2012 **21** 552–557. (<https://doi.org/10.1097/BPB.0b013e328355e5f1>)
- 50. Waisbrod G, Schiebel F & Beck M.** Abnormal femoral antetorsion—a subtrochanteric deformity. *Journal of Hip Preservation Surgery* 2017 **4** 153–158. (<https://doi.org/10.1093/jhps/hnx013>)
- 51. Batailler C, Weidner J, Wyatt M, Dalmay F & Beck M.** Position of the greater trochanter and functional femoral antetorsion: which factors matter in the management of femoral antetorsion disorders? *Bone and Joint Journal* 2018 **100-B** 712–719. (<https://doi.org/10.1302/0301-620X.100B6.BJJ-2017-1068.R1>)
- 52. Albers CE, Rogers P, Wambeek N, Ahmad SS, Yates PJ & Prosser GH.** Preoperative planning for redirective, periacetabular osteotomies. *Journal of Hip Preservation Surgery* 2017 **4** 276–288. (<https://doi.org/10.1093/jhps/hnx030>)
- 53. Markhardt BK, Beilfuss MA, Hetzel SJ, Goodspeed DC & Spiker AM.** 3D-printed models for periacetabular osteotomy surgical planning. *Journal of Hip Preservation Surgery* 2020 **7** 748–754. (<https://doi.org/10.1093/jhps/hnab024>)